

Article

Pyridyl Methylsulfinyl Benzimidazole Derivatives as Promising Agents against *Giardia lamblia* and *Trichomonas vaginalis*

Beatriz Hernández-Ochoa ^{1,2}, Víctor Martínez-Rosas ^{1,3} , Laura Morales-Luna ^{3,4}, Ernesto Calderón-Jaimes ², Luz María Rocha-Ramírez ⁵ , Daniel Ortega-Cuellar ⁶ , Yadira Rufino-González ⁷ , Abigail González-Valdez ⁸, Roberto Arreguin-Espinosa ⁹ , Sergio Enríquez-Flores ¹⁰ , Rosa Angélica Castillo-Rodríguez ¹¹ , Noemí Cárdenas-Rodríguez ¹² , Carlos Wong-Baeza ¹³ , Isabel Baeza-Ramírez ¹³ and Saúl Gómez-Manzo ^{3,*} 

- ¹ Programa de Posgrado en Biomedicina y Biotecnología Molecular, Escuela Nacional de Ciencias Biológicas, Instituto Politécnico Nacional, Mexico City 11340, Mexico
 - ² Laboratorio de Inmunología, Hospital Infantil de México Federico Gómez, Secretaría de Salud, Mexico City 06720, Mexico
 - ³ Laboratorio de Bioquímica Genética, Instituto Nacional de Pediatría, Secretaría de Salud, Mexico City 04530, Mexico
 - ⁴ Posgrado en Ciencias Biológicas, Universidad Nacional Autónoma de México, Mexico City 04510, Mexico
 - ⁵ Unidad de Investigación en Enfermedades Infecciosas, Hospital Infantil de México Federico Gómez, Dr. Márquez No. 162, Colonia Doctores, Mexico City 06720, Mexico
 - ⁶ Laboratorio de Nutrición Experimental, Instituto Nacional de Pediatría, Secretaría de Salud, Mexico City 04530, Mexico
 - ⁷ Laboratorio de Parasitología Experimental, Instituto Nacional de Pediatría, Secretaría de Salud, Mexico City 04530, Mexico
 - ⁸ Departamento de Biología Molecular y Biotecnología, Instituto de Investigaciones Biomédicas, Universidad Nacional Autónoma de México, Mexico City 04510, Mexico
 - ⁹ Departamento de Química de Biomacromoléculas, Instituto de Química, Universidad Nacional Autónoma de México, Mexico City 04510, Mexico
 - ¹⁰ Laboratorio de Biomoléculas y Salud Infantil, Instituto Nacional de Pediatría, Secretaría de Salud, Mexico City 04530, Mexico
 - ¹¹ CICATA Unidad Morelos, Instituto Politécnico Nacional, Boulevard de la Tecnología, 1036 Z-1, P 2/2, Atlacholoaya, Xochitepec 62790, Mexico
 - ¹² Laboratorio de Neurociencias, Instituto Nacional de Pediatría, Secretaría de Salud, Mexico City 04530, Mexico
 - ¹³ Laboratorio de Biomembranas, Departamento de Bioquímica, Escuela Nacional de Ciencias Biológicas, Instituto Politécnico Nacional, Mexico City 11340, Mexico
- * Correspondence: saulmanzo@ciencias.unam.mx; Tel.: +52-55-1084-0900 (ext. 1442)



Citation: Hernández-Ochoa, B.; Martínez-Rosas, V.; Morales-Luna, L.; Calderón-Jaimes, E.; Rocha-Ramírez, L.M.; Ortega-Cuellar, D.; Rufino-González, Y.; González-Valdez, A.; Arreguin-Espinosa, R.; Enríquez-Flores, S.; et al. Pyridyl Methylsulfinyl Benzimidazole Derivatives as Promising Agents against *Giardia lamblia* and *Trichomonas vaginalis*. *Molecules* **2022**, *27*, 8902. <https://doi.org/10.3390/molecules27248902>

Academic Editor: Irini Doytchinova

Received: 23 November 2022

Accepted: 11 December 2022

Published: 14 December 2022

Publisher's Note: MDPI stays neutral with regard to jurisdictional claims in published maps and institutional affiliations.



Copyright: © 2022 by the authors. Licensee MDPI, Basel, Switzerland. This article is an open access article distributed under the terms and conditions of the Creative Commons Attribution (CC BY) license (<https://creativecommons.org/licenses/by/4.0/>).

Abstract: Protozoan parasites, such as *Giardia lamblia* and *Trichomonas vaginalis*, cause the most prevalent infections in humans in developing countries and provoke significant morbidity and mortality in endemic countries. Despite its side-effects, metronidazole is still the drug of choice as a giardiocidal and trichomonacidal tissue-active agent. However, the emergence of metronidazole resistance and its evolved strategies of parasites to evade innate host defenses have hindered the identification and development of new therapeutic strategies against these parasites. Here, we tested five synthesized benzimidazole derivatives as possible drugs for treating giardiasis and trichomoniasis, probing the bifunctional enzyme glucose 6-phosphate dehydrogenase::6-phosphogluconolactone from *G. lamblia* (GIG6PD::6PGL) and *T. vaginalis* (TvG6PD::6PGL) as a drug target. The investigated benzimidazole derivatives were H-B2M1, H-B2M2, H₂N-BZM6, O₂N-BZM7, and O₂N-BZM9. The recombinant enzymes were used in inhibition assays, and in silico computational predictions and spectroscopic studies were applied to follow the structural alteration of the enzymes and identify the possible mechanism of inhibition. We identified two potent benzimidazole compounds (O₂N-BZM7 and O₂N-BZM9), which are capable of inhibiting both protozoan G6PD::6PGL enzymes and in vitro assays with these parasites, showing that these compounds also affect their viability. These results demonstrate that other therapeutic targets of the compounds are the enzymes GIG6PD::6PGL and TvG6PD::6PGL, which contribute to their antiparasitic effect and their possible use in anti-giardial and trichomonacidal therapies.

Keywords: anti-giardial; antitrichomonal; benzimidazole derivatives; inhibition; enzymes

1. Introduction

Infections caused by parasites represent a significant public health crisis in developing countries [1]. In recent years, different strategies have been used in the search for new treatments against protozoan parasites of medical importance, such as *G. lamblia* and *T. vaginalis*. Currently, drug discovery strategies are principally based on identifying essential biomolecules of pharmacological interest which, after inhibiting its activity/function, could be lethal to the parasite. Parasite metabolic pathways provide an attractive target for drug development and are, therefore, of particular interest [2]. For example, it has been shown that the disruption of the glycolysis via the inhibition of triosephosphate isomerase enzyme (TIM) affects the viability of *G. lamblia*, suggesting that this enzyme is identified as a pharmacological target [3,4]. A similar effect was observed by several compounds that selectively inhibit the TIM of *T. vaginalis* [5,6]. Additionally, the repurposing of drugs is an attractive pharmacological strategy for new therapeutics [7].

Over the years, benzimidazole compounds have received considerable attention in chemistry medicinal owing to their wide biological activities and diverse therapeutic applications. Thus, benzimidazole derivatives are crucial structural scaffolds found in diverse libraries of biologically active compounds which are therapeutically useful agents in drug discovery and medicinal research. Numerous compounds containing benzimidazole moieties have been reported to exhibit diverse biological and pharmacological properties, including analgesic, antibacterial, anticancer, and antiparasitic activities.

In this scenario, the commercial drug omeprazole (derived from pyridyl methanesulfinyl benzimidazole) has been suggested as an anti-giardial compound, since it selectively inactivates the triosephosphate isomerase of *G. lamblia* (GITIM) by chemical modification of cysteine residues, which leads to the parasite's death [8]. In addition, some other proton pump inhibitors (PPIs) are reported to be active against *Giardia* trophozoites in vitro in the range of effectivity for albendazole [4,9,10]. On the basis of the above, we previously designed and synthesized five compounds analogous to omeprazole (Figure 1), 2-[(pyridin-2-yl)methanesulfinyl]-1*H*-benzimidazole (**H-BZM1**), 2-[(4-methoxy-3,5-dimethylpyridin-2-yl)methanesulfinyl]-1*H*-benzimidazole (**H-BZM2**), 2-[[3-methyl-4-(2,2,2-trifluoroethoxy)pyridin-2-yl]methanesulfinyl]-1*H*-benzimidazol-6-amine (**H₂N-BZM6**), 6-nitro-2-[(pyridin-2-yl)methanesulfinyl]-1*H*-benzimidazole (**O₂N-BZM7**), and 2-[[3-methyl-4-(2,2,2-trifluoroethoxy)pyridin-2-yl]methanesulfinyl]-6-nitro-1*H*-benzimidazole (**O₂N-BZM9**) [11], whose difference lies in different substituent groups linked to the benzimidazole and pyridine ring and enhances the anti-giardial activity of omeprazole through the inhibition of the GITIM enzyme. Notably, the previously analyzed compounds with the most anti-giardial activity were **O₂N-BZM7** and **O₂N-BZM9**. These compounds also showed a low cytotoxicity in Caco-2 and HT29 cell lines; however, whether these compounds have another protozoan or protein target needs to be evaluated.

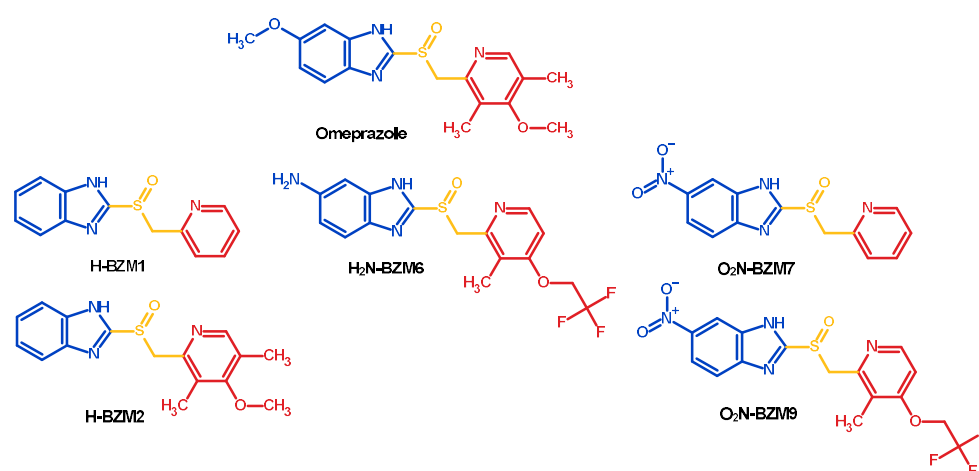


Figure 1. Chemical structure of pyridyl methylsulfinyl benzimidazole compounds analogous to omeprazole; the benzimidazole and pyridine core are shown in blue and red color.

The aforementioned results allowed the optimization of the anti-giardial activity of omeprazole-like compounds through chemical modifications and, thus, identification of two compounds with greater anti-giardial activity and with the potential to inhibit GITPI. However, there is increasing evidence that a drug interacts with various molecular targets. For example, it has been reported that omeprazole binds to multiple proteins and can form highly stable complexes that are not dependent on disulfide linkages between the drug and protein targets [12]. Therefore, it was of our interest to study the bifunctional enzyme glucose 6-phosphate dehydrogenase::6-phosphogluconolactone (G6PD::6PGL) as a possible drug target. This enzyme is involved in the pentose phosphate pathway and provides the parasite with NADPH and ribose molecules, which are essential for the survival of most protozoans. They are also a possible biomolecule target for benzimidazole compounds, which could contribute to giardiacidal and trichomonocidal activities through the inhibition of G6PD::6PGL.

On the basis of the above, in this study, we analyzed the effect of **H-BZM1**, **H-BZM2**, **H₂N-BZM6**, **O₂N-BZM7**, and **O₂N-BZM9** compounds on the enzyme G6PD::6PGL from *G. lamblia* (GIG6PD::6PGL) and *T. vaginalis* (TvG6PD::6PGL) to demonstrate the ability of the compounds to inactivate these enzymes. We found that compounds **O₂N-BZM7** and **O₂N-BZM9** have the most promising effects against giardiasis and trichomoniasis since they inactivate the G6PD::6PGL enzymes of both parasites, alter their structures, and efficiently cause the death of *G. lamblia* and *T. vaginalis* trophozoites.

2. Results and Discussion

2.1. In Vitro Screening of GIG6PD:6PGL and TvG6PD:6PGL Inactivation with Benzimidazole Compounds

Previously, it was reported that omeprazole and PPI analogs exhibit anti-giardial activity because these compounds act as inhibitors of the glycolytic enzyme GITIM by covalently binding to cysteine residues [4,10]. In this sense, Hernandez-Ochoa et al. [11], with the aim of enhancing the anti-giardiasis activity of omeprazole, synthesized and probed the anti-giardial effect of five new pyridyl methylsulfinyl benzimidazole compound omeprazole analogs, named **H-BZM1**, **H-BZM2**, **H₂N-BZM6**, **O₂N-BZM7**, and **O₂N-BZM9**. Thus, it was determined that one of the pharmacological targets of these compounds is the glycolytic enzyme GITIM, although it cannot be the only target. Therefore, it is in our interest to know if these compounds with inhibitory capacities in GITIM also have the capability to inhibit the fused recombinant G6PD::6PGL enzymes from *G. lamblia* and *T. vaginalis*.

It is important to mention that these compounds are structural analogs to proton pump inhibitors; they maintain the core of a substituted benzimidazole ring joined to a substituted pyridine linked by a methylsulfinyl chain and, thus, they are chiral compounds.

In this work, all the assays were carried out with the racemic mixture of each one of the compounds (R and S enantiomers). To determine the inhibitory effect of benzimidazole compounds on the activity of the fused enzymes, a general assay was performed using 400 μM of each compound. Table 1 shows the inactivation results for both enzymes; we observed that these compounds showed an inhibitory activity in the enzymes to different degrees of inactivation. The complete activity of the GIG6PD::6PGL enzyme was eradicated by four compounds (**H-BZM2**, **H₂N-BZM6**, **O₂N-BZM7**, and **O₂N-BZM9**), while the **H-BZM1** compound inhibited only a 62% activity. This demonstrates that the fused enzyme GIG6PD::6PGL is totally inactivated with benzimidazole compounds. On the other hand, the enzyme TvG6PD::6PGL was only inhibited with **O₂N-BZM7** and **O₂N-BZM9** compounds by 95% and 72%, respectively, while the other three compounds inhibited the enzyme activity by less than 50%.

Table 1. Percentage of enzyme activity of GIG6PD::6PGL and TvG6PD::6PGL after incubation at 37 °C for 2 h with benzimidazole derivative compounds of 400 μM .

Compounds	Inhibition (%) at 400 μM of GIG6PD::6PGL *	Inhibition (%) at 400 μM of TvG6PD::6PGL *
H-BZM1	62 \pm 5	7 \pm 5
H-BZM2	100 \pm 5	47 \pm 5
H₂N-BZM6	100 \pm 5	12 \pm 5
O₂N-BZM7	100 \pm 5	95 \pm 5
O₂N-BZM9	100 \pm 5	72 \pm 5

* The results are relative to the control (enzyme without inhibitor).

Our results support previous research on GITIM inhibition, where the best compounds with anti-giardial activity were **H-BZM2**, **O₂N-BZM7**, and **O₂N-BZM9** [11]. Therefore, we decided to use **H-BZM2**, **O₂N-BZM7**, and **O₂N-BZM9** compounds for further assays on the fused enzyme GIG6PD::6PGL. On the other hand, **O₂N-BZM7** and **O₂N-BZM9** compounds were used with the TvG6PD::6PGL enzyme for presenting and inhibition percentage superior to 70%.

To calculate the concentration of compound needed to inactivate 50% of the activity of the GIG6PD::6PGL and TvG6PD::6PGL enzymes, inactivation assays were performed using appropriate concentrations of the compounds. Figure 2A shows the residual activity of the GIG6PD::6PGL enzyme after incubation with the benzimidazole compounds. It was observed that, as the concentration of each compound increases, the residual activity of the enzyme decreases. In fact, the exposure of the GIG6PD::6PGL enzyme to **H-BZM2**, **O₂N-BZM7**, and **O₂N-BZM9** induced the abolition of enzyme activity in a similar way. In this regard, the enzyme lost 100% of its activity when incubated with 100 μM of **H-BZM2** and **O₂N-BZM9**, whereas **O₂N-BZM7** seems to be more effective and requires a lower concentration (60 μM) to eradicate enzyme activity. We also evaluated the IC_{50} and found that **O₂N-BZM7** was more effective as the concentration required to reduce GIG6PD::6PGL enzyme activity by 50% was 11 μM , whereas, for **H-BZM2** and **O₂N-BZM9**, the IC_{50} values were 24 μM and 15 μM , respectively (Figure 2A).

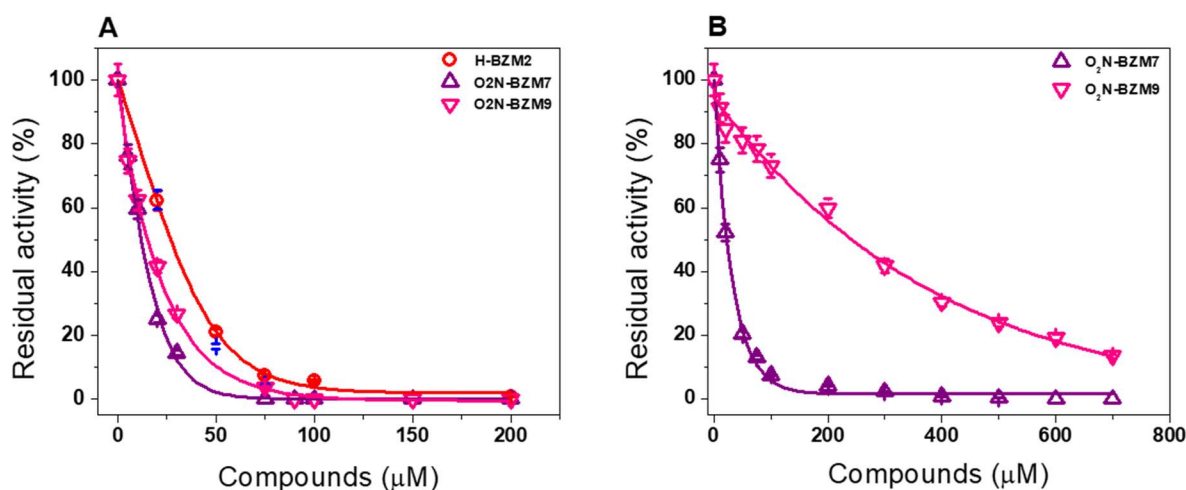


Figure 2. G6PD::6PGL enzyme inactivation assays with compounds. Effect of compounds **H-BZM2**, **O₂N-BZM7**, and **O₂N-BZM9** on (A) GIG6PD::6PGL and (B) TvG6PD::6PGL. The protein was adjusted to a concentration of 0.2 mg/mL and incubated with increasing concentrations of each compound for 2 h at 37 °C. At the end of the incubation time, residual activity was measured. Results are shown as the mean values of three independent tests.

With respect to TvG6PD::6PGL enzyme, **O₂N-BZM7** showed an IC₅₀ value of 22 μM, while the compound of **O₂N-BZM9** had an 11-fold higher IC₅₀ value (240 μM) (Figure 2B). It is interesting to note that these two compounds have a nitro group (NO₂) in position 5 of the benzimidazole ring, suggesting that the NO₂ is an essential cause of the potent inhibitory effect on enzymes. On the other hand, compound **O₂N-BZM7** has only hydrogen atoms in the pyridine ring, whereas **O₂N-BZM9** has a methyl group and a trifluoroethoxy group, suggesting that these large groups probably affect the interaction of this compound with the enzyme. A similar effect was also observed for the enzyme GIG6PD::6PGL, where compound **O₂N-BZM7** showed a lower IC₅₀ value than compound **O₂N-BZM9**.

Lastly, it is interesting to mention that **H-BZM2**, **O₂N-BZM7**, and **O₂N-BZM9** compounds presented a better inactivation in the G6PD::6PGL-fused enzyme from *G. lamblia* regarding the TIM enzyme from the same organism, where IC₅₀ values of 37 μM, 12 μM, and 20 μM were reported, respectively [11]. Moreover, **O₂N-BZM7** and **O₂N-BZM9** compounds showed a better inactivation profile in the fused enzyme from *G. lamblia* regarding TvG6PD::6PGL, suggesting a probable selectivity inhibition of these compounds in the fused enzyme of *G. lamblia* with respect to the enzyme of *T. vaginalis*.

2.2. Second-Order Rate Constant (k_2) of Selected Compounds

To determine the reactivity of chemical compounds on the GIG6PD::6PGL and TvG6PD::6PGL enzymes, second-order inactivation rate constants (k_2) were calculated. The k_2 constant represents the rate of formation of the enzyme–inhibitor complex. In Figure 3A–C, we can see that the inactivation of GIG6PD::6PGL enzyme by the chemical compounds exhibits the behavior of a pseudo-first-order inactivation. Thereafter, the calculated k_1 values were plotted versus the chemical compound concentrations, and the second-order inactivation rate constant (k_2) was calculated. The calculated k_2 values for **H-BZM2**, **O₂N-BZM7**, and **O₂N-BZM9** were 3.3, 1.9, and 6.1 M⁻¹·s⁻¹, respectively (Figure 3D,E,F). These results suggest that the **O₂N-BZM9** compound rapidly forms an inhibitor–enzyme complex, followed by **O₂N-BZM7** and **H-BZM2**. Moreover, these results show that the enzyme G6PD::6PGL of *G. lamblia* is also an efficient target of these compounds, which potentially contributes to their anti-giardial activity since they effectively form an inhibitor–enzyme complex with the GIG6PD::6PGL enzyme.

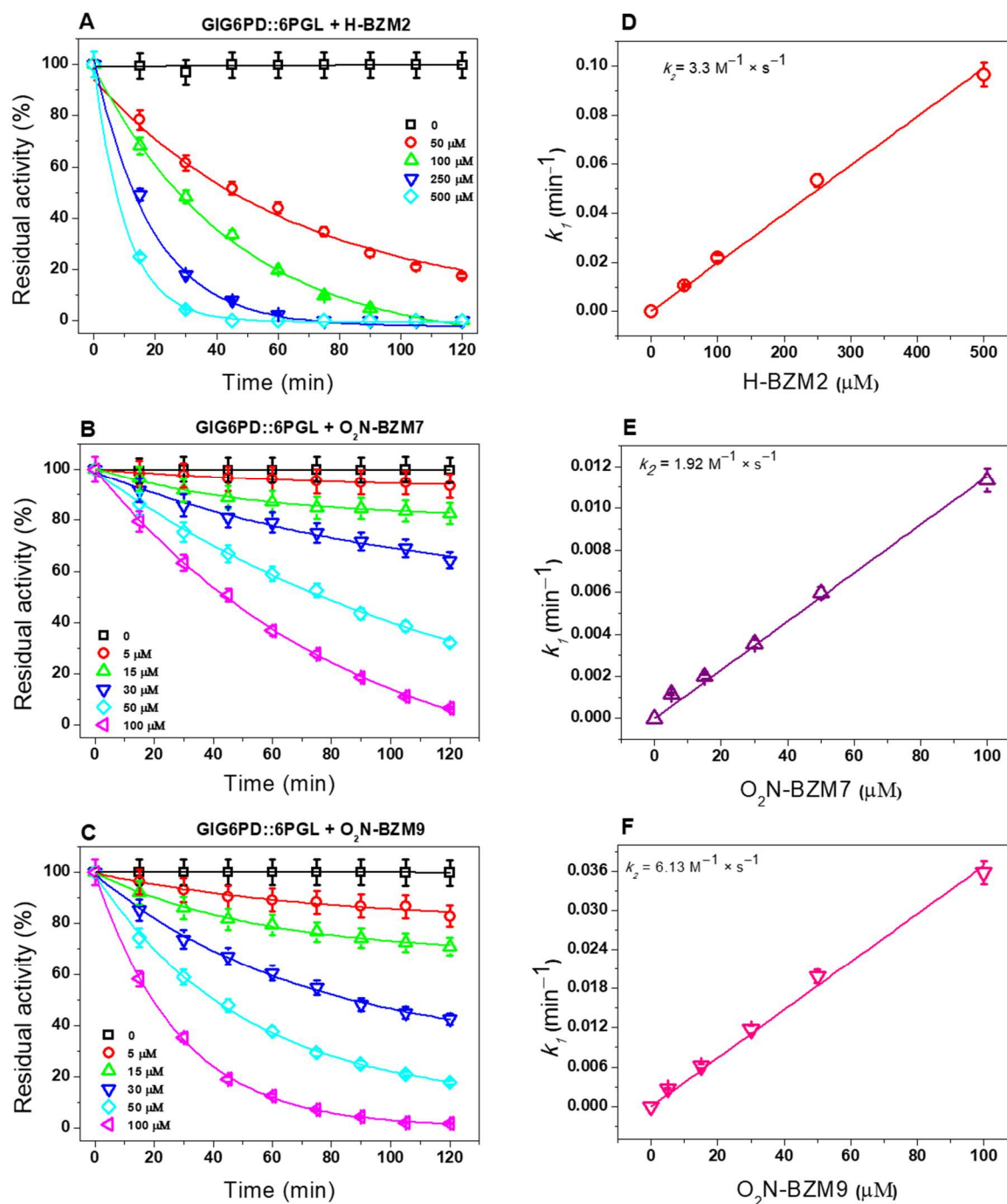


Figure 3. Inactivation assays of G6PD::6PGL enzyme form *G. lamblia* with H-BZM2, O₂N-BZM7, and O₂N-BZM9. (A–C) Pseudo-first-order rate constants (k_1) for each compound were calculated by fitting the data to the exponential decay equation $A_R = A_0 e^{-k_1 t}$, where A_0 is the initial activity value. All the experiments were performed in triplicate; the bars represent the standard error. (D–F) Second-order inactivation rate constants (k_2) were obtained by plotting k_1 values against compound concentrations and fitted to a linear regression model. All experiments were performed in triplicate; standard errors were less than 5%.

Previously, it was reported that O₂N-BZM7 and O₂N-BZM9 compounds presented k_2 values of $3.2 \text{ M}^{-1} \cdot \text{s}^{-1}$ and $2.8 \text{ M}^{-1} \cdot \text{s}^{-1}$ over the inactivation of GITIM enzyme [11]. Therefore, these results demonstrate the great ability of the O₂N-BZM7 and O₂N-BZM9 compounds to form an enzyme–inhibitor complex with the GIG6PD::6PGL and TIM enzymes from *G. lamblia*, which contributes to the anti-giardial effect of the compounds.

Regarding the TvG6PD::6PGL enzyme, the highest reactivity was shown by the compound **O₂N-BZM9** with a k_2 value of $1.62 \text{ M}^{-1} \cdot \text{s}^{-1}$ (Figure 4B,D), which is twice the value determined for **O₂N-BZM7** ($0.85 \text{ M}^{-1} \cdot \text{s}^{-1}$) (Figure 4A,C). It is interesting to note that, when we compared the k_2 values for TvG6PD::6PGL with the k_2 value for the enzyme GlG6PD::6PGL (Table 2), **O₂N-BZM7** and **O₂N-BZM9** compounds formed an enzyme–inhibitor complex faster with the fused enzyme of *G. lamblia* compared to the enzyme of *T. vaginalis*, which suggests a species-specific inhibition of the compounds toward the enzyme GlG6PD::6PGL.

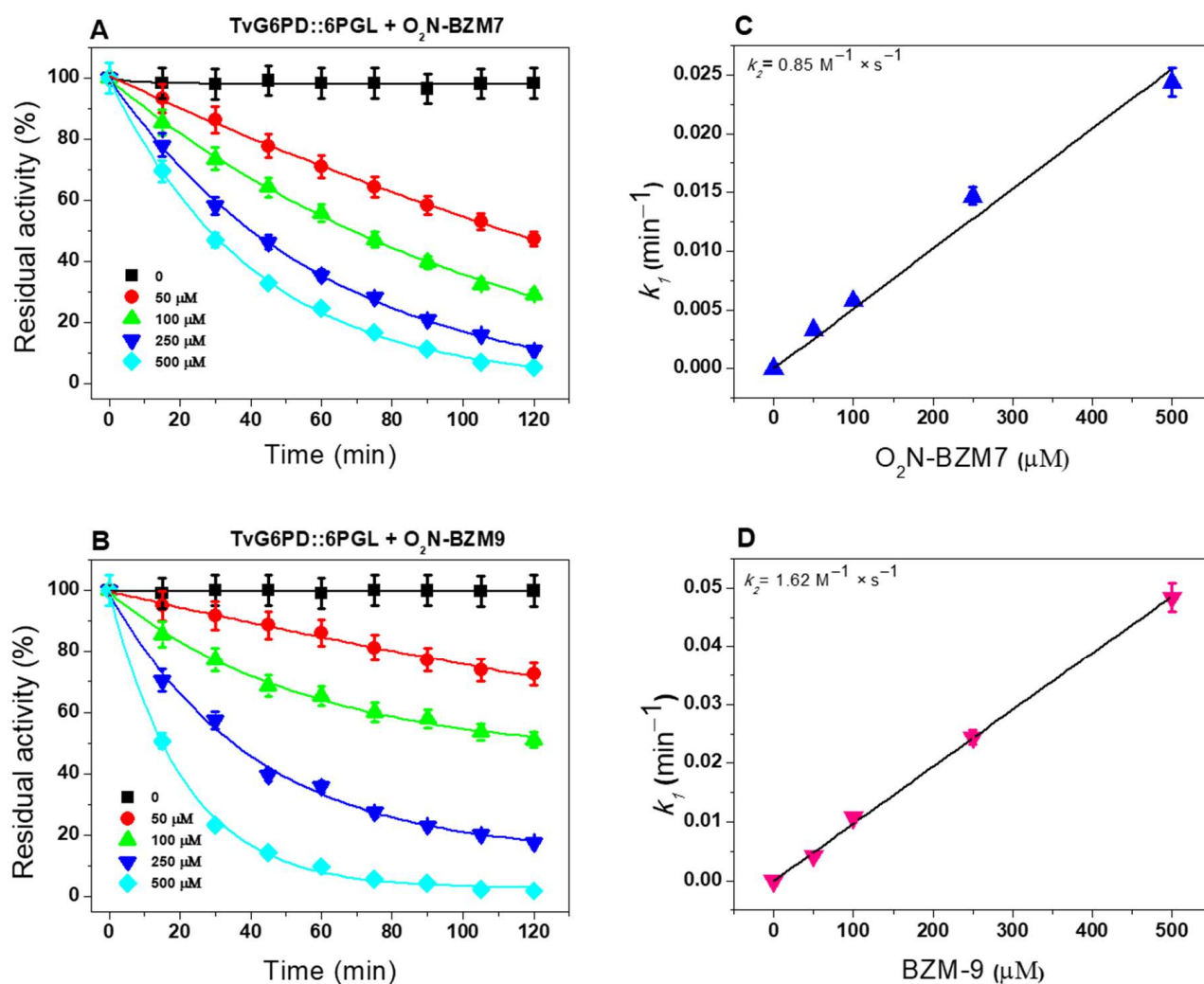


Figure 4. Inactivation assays of the enzyme G6PD::6PGL of *T. vaginalis* with **O₂N-BZM7** and **O₂N-BZM9**. (A,B) Pseudo-first-order rate constants (k_1) for each compound were calculated by fitting the data to the exponential decay equation $A_R = A_0 e^{-kt}$, where A_0 is the initial activity value. (C,D) Second-order inactivation rate constants (k_2) were obtained by plotting k_1 values against compound concentrations and fitted to a linear regression model. All experiments were performed in triplicate; standard errors were less than 5%.

Table 2. Summary of inhibition, IC₅₀ values, and second-order rate constant values of inactivation (k_2) of the compounds analyzed in this study.

Compounds	GIG6PD::6PGL			TvG6PD::6PGL		
	Inhibition (%)	IC ₅₀ (μM)	k_2 (M ⁻¹ ·s ⁻¹)	Inhibition (%)	IC ₅₀ (μM)	k_2 (M ⁻¹ ·s ⁻¹)
H-BZM2	100	24	3.3	47.5	-	-
O ₂ N-BZM7	100	11	1.9	94.9	22	0.8
O ₂ N-BZM9	100	15	6.1	71.9	240	1.6

Lastly, it is important to mention that the evaluated **O₂N-BZM7** and **O₂N-BZM9** compounds show a high inhibitory potential in the GIG6PD::G6PD enzyme compared to the results previously reported by Martínez-Rosas et al. [13]. In that report, the authors investigated the impact of an in-house chemical library of 55 compounds on the activity of the fused TvG6PD::6PGL protein and found four compounds—JMM-3, CNZ-3, CNZ-17, and MCC-7—that inhibited the TvG6PD::6PGL protein; however, the calculated k_2 values were 0.33, 0.66, 0.38, and 0.26 M⁻¹·s⁻¹, respectively.

2.3. Spectroscopic and Chromatographic Characterization

To determine the mechanism probability of inactivation by the chemical compounds on the fused G6PD::6PGL from *G. lamblia* and *T. vaginalis*, alterations in secondary, tertiary structure, and quaternary structure were determined in the presence of **O₂N-BZM7** and **O₂N-BZM9** chemical compounds since they presented a better inactivation profile in both proteins, with lower IC₅₀ values, and rapidly formed the inhibitor-enzyme complex.

2.3.1. Circular Dichroism Experiments

Firstly, we examined changes in the secondary structure by the circular dichroism (CD) signal of GIG6PD::6PGL and TvG6PD::6PGL proteins in the absence of the benzimidazole compound, which was used as a control. Then, CD spectra of the enzymes were determined after the incubation with the compounds at the IC₅₀ concentration. As seen in Figure 5, no significant changes were observed in the presence of the compounds in the fused G6PD::6PGL proteins from *G. lamblia* and *T. vaginalis*. The **O₂N-BZM7** and **O₂N-BZM9** chemical compounds did not induce alterations of the secondary structure, as indicated by the similarity of the CD spectra of the GIG6PD::6PGL enzyme without compounds. On the basis of these results, we suggest that the loss of activity can be given at the level of tertiary and/or quaternary structure. Lastly, it is interesting to mention that, in the study carried out by Hernández-Ochoa et al. (2020) [11] with the same compounds in the enzyme TIM from *G. lamblia*, it was found that these same compounds showed a negative effect on the secondary structure of GITIM. This difference in the alterations in the secondary structure could indicate that the inactivation mechanism is different from that previously reported in the GITIM, where the sulfur atom of the benzimidazole ring forms a covalent bond with the cysteine residues present in the TIM protein from *G. lamblia* [11].

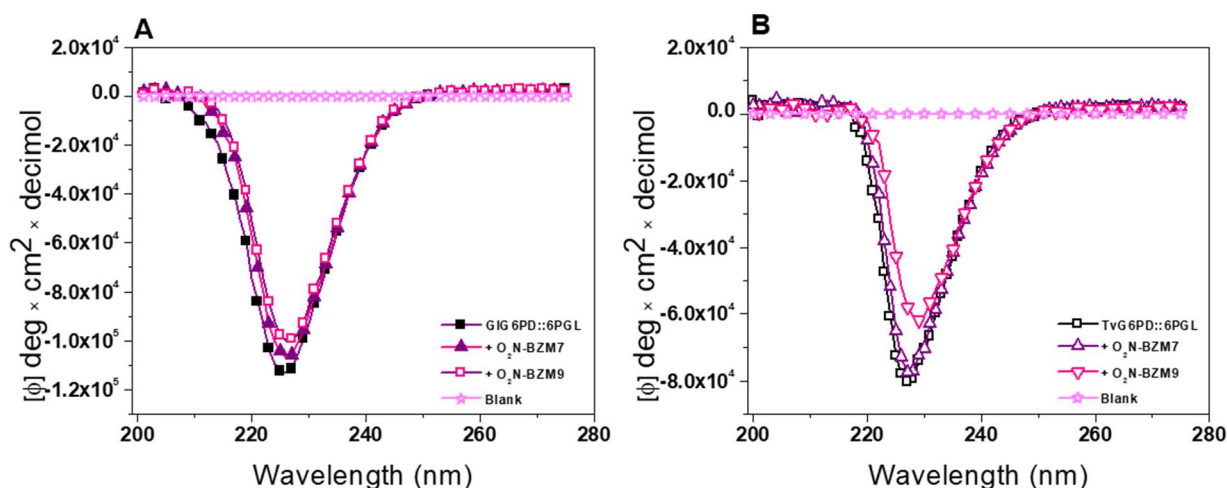


Figure 5. Spectroscopic characterization of enzymes. (A) Far-ultraviolet circular dichroism (CD) spectra of the enzyme GIG6PD::6PGL and (B) TvG6PD::6PGL. Changes in molar ellipticity were monitored by circular dichroism. The protein was adjusted to 0.5 mg/mL in 50 mM phosphate buffer and incubated with the benzimidazole compounds at the IC_{50} concentration of each inhibitor for 2 h at 37 °C before measuring. The results shown are representative of triplicate experiments.

2.3.2. Intrinsic Fluorescence Assays

Changes in the tertiary structure and global stability of the fused G6PD::6PGL protein from *G. lamblia* and *T. vaginalis* were evaluated by monitoring the intrinsic fluorescence properties of the eight tryptophan residues contained in the GIG6PD::6PGL/monomer and the nine tryptophan residues of the TvG6PD::6PGL/monomer. Regarding fused G6PD::6PGL from *G. lamblia*, we observed that the two compounds presented a lower intrinsic fluorescence intensity of G6PD::6PGL protein with respect to the control (Figure 6A). The intrinsic fluorescence of the native GIG6PD::6PGL protein without inhibitors showed a peak at 344 nm with a maximum intensity of 874 arbitrary units (a.u.), while both **O₂N-BZM7** and **O₂N-BZM9** chemical compounds showed the highest negative effects with a maximum fluorescence intensity of 329 a.u., indicating a reduction of 62% compared to the control. These results are in agreement with those previously observed for the TIM enzyme from *G. lamblia*, where a decrease in fluorescence intensity with these two compounds was also observed [11].

Regarding the intrinsic fluorescence intensity of fused TvG6PD::6PGL protein from *T. vaginalis*, we observed that **O₂N-BZM9** decreases 84% of intrinsic protein fluorescence (102 a.u.) with respect to the native protein (673 a.u.), while **O₂N-BZM7** showed a maximal fluorescence intensity of 415 a.u, indicating a reduction of 30% compared to the TvG6PD::6PGL enzyme without compounds (Figure 6B). Interestingly, a redshift was observed in the presence of **O₂N-BZM9**, suggesting the exposure of the solvent to previously buried hydrophobic regions. Moreover, the two benzimidazole compounds affect the fused G6PD::6PGL proteins of the native parasite, indicating that the compounds caused a rearrangement in the microenvironment of the tryptophan residues after the incubation with the compounds.

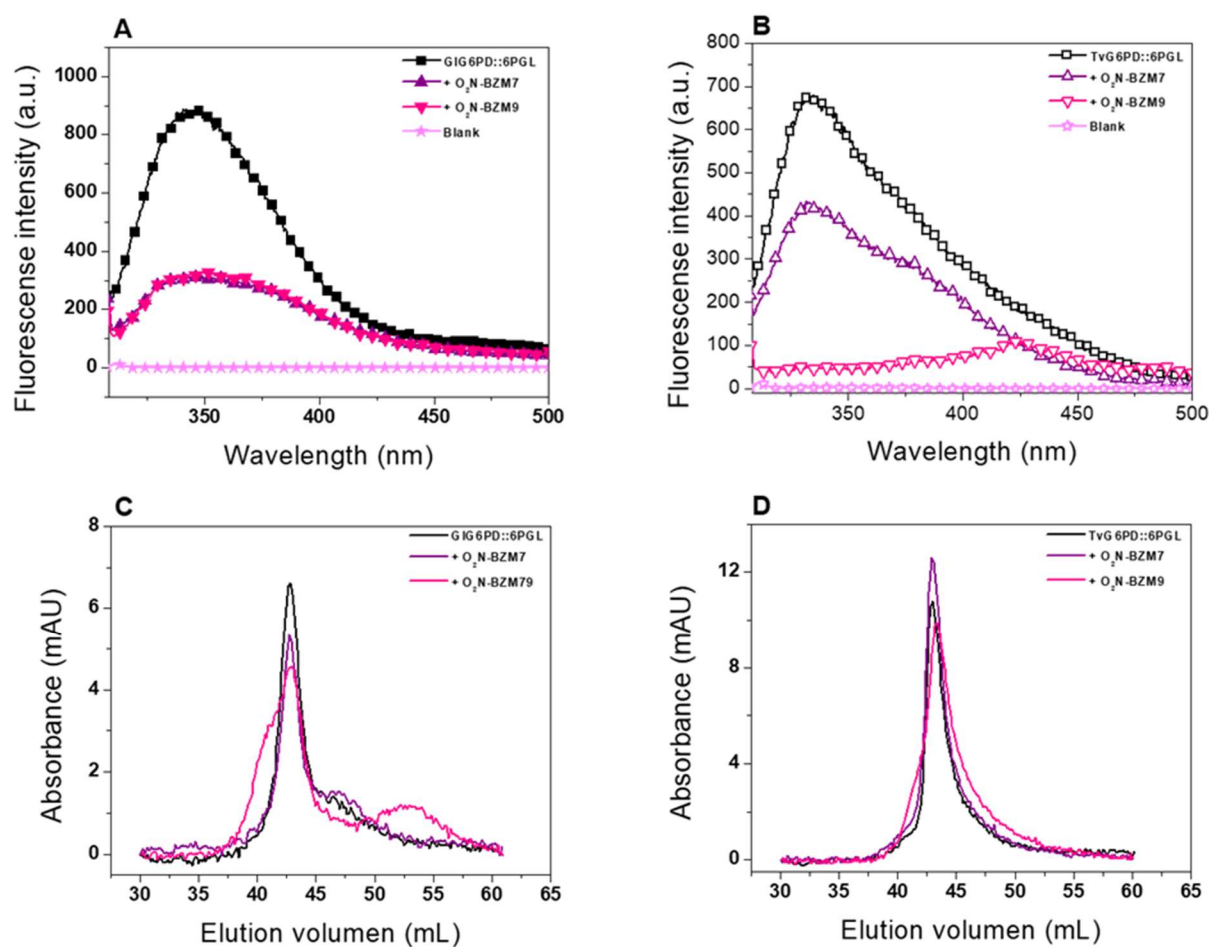


Figure 6. Spectroscopic and chromatographic characterization. (A) Intrinsic fluorescence emission spectra of GIG6PD::6PGL enzyme and (B) TvG6PD::6PGL in the absence and presence of the benzimidazole compounds. The values obtained from the buffer without protein corresponded to the blank and were subtracted from the spectra obtained with protein. Data are presented as the mean of three experiments. (C) Gel filtration chromatography of GIG6PD::6PGL and (D) TvG6PD::6PGL in the absence or presence of the compounds. The enzymes (0.5 mg/mL) were incubated at 37 °C for 2 h with each of the benzimidazole compounds and then loaded onto a Sephacryl TMS-200 HR HiPrep™ 16/60 column.

Lastly, we evaluated the changes in the quaternary structure using size exclusion chromatography. As seen in Figure 6C,D, no significant changes were observed in the retention time in the fused G6PD::6PGL protein from *G. lamblia* and *T. vaginalis* in the absence and presence of compounds, indicating that both enzymes were eluted as single peaks with retention volumes corresponding to native tetramers. These results suggest that the inactivation of fused proteins by benzimidazole compounds does not alter the dimeric structure of the enzyme and induces local modifications of the tridimensional structure instead of global alterations.

The spectroscopic and chromatographic results indicate that benzimidazole compounds alter the tridimensional structure of the proteins, resulting in a loss of catalytic activity in both fused enzymes. Furthermore, these results are correlated with the loss of catalytic activity and are in accordance with biochemical assays, in which the benzimidazole O₂N-BZM9 compound formed the enzyme–inhibitor complex faster than O₂N-BZM7.

2.4. Molecular Docking Study

Since the complete 3D structure of G6PD::6PGL of *G. lamblia* and *T. vaginalis* is still unknown, the models generated by Morales-Luna et al. 2018 [14] and Martinez-Rosas et al. [13] were used to identify probable interaction zones for compounds, and the (R) and (S) enantiomers of the **O₂N-BZM7** and **O₂N-BZM9** compounds were used for the blind docking analysis. The docking performed on the entire surface of the homodimer indicated that both (R) and (S) enantiomers of the compounds specifically bind to the G6PD domain of the fused enzyme. They do not bind near any cysteine residue present in this domain, and both (R) and (S) enantiomers of each compound have almost the same binding affinity. Representative binding sites for each compound are shown in Figure 7A–H. This analysis allowed us to know the probable binding zones of the compounds; however, as has been reported, the molecular coupling method is not reliable to accurately predict the preference of the targets for the R or S enantiomers [15].

It is interesting to note that the compounds do not bind near any cysteine residue of the G6PD domain; these results are in concordance with the previously reported by Cartee and Wang [12], where they identified the binding of omeprazole to protein targets by monoclonal antibodies and concluded that omeprazole binds to multiple proteins and is capable of forming highly stable complexes that are not dependent on disulfide linkages between the drug and protein targets.

The docking analysis revealed a pocket of interaction in both enzymes for the two compounds, whose zone is near the catalytic site. In this pocket, interactions between the compounds and amino acids that participate in the correct positioning of catalytic NADP⁺ were identified. In the case of the compound **(R)-O₂N-BZM7** and the enzyme GIG6PD::6PGL, it was identified that two H-bonds are formed between the sulfoxide group of the compound and the amino acids Arg46 and Ser14; the amino acid Ser14 is part of the hexapeptide conserved (GxxGGDLA) in the G6PD's enzymes, whose function is the correct positioning of the catalytic NADP⁺ [16] (Figure 8A), and the most stable conformer showed a ΔG of -7.11 kcal/mol. Regarding **(R)-O₂N-BZM9**, it showed a binding energy of -8.34 kcal/mol and formed one H-bond between the sulfoxide group of the compound and Arg230, as well as two H-bonds between the nitro group, and Glu223 and Tyr186 (Figure 8C). This last amino acid is found in the conserved sequence 182-RIDHYLGKE-190 (the amino acid number corresponding to GIG6PD::6PGL sequence) [17]. Additionally, Glu233 is important for G6P binding and defining the shape of the binding site [18]. Another zone of interaction in GIG6PD::6PGL was near the structural NADP⁺ binding site, where **(R)-O₂N-BZM7** showed a ΔG of -8.45 kcal/mol and formed one H-bond with the sulfoxide group and Asp362 (Figure 8E), while **(R)-O₂N-BZM9** formed three H-bonds with the nitro group and Arg352 and one H-bond with benzimidazole ring and Tyr707, with an energy binding of -8.63 kcal/mol (Figure 8G). Similar results were found with the (S) enantiomer of **O₂N-BZM7** and **O₂N-BZM9** compounds (Figure 8B,D,F,H). These results show that **O₂N-BZM9** has a more favorable binding energy than **O₂N-BZM7** in both zones, and, according to the determined inhibition constant k_2 , **O₂N-BZM9** ($6.13 \text{ M}^{-1}\cdot\text{s}^{-1}$) is able to inhibit the enzyme faster than **O₂N-BZM7** (k_2 of $1.92 \text{ M}^{-1}\cdot\text{s}^{-1}$). In addition, the most stable conformer in the catalytic pocket is positioned very close to the nicotinamide ring of NADP⁺, which is the receptor for electrons and protons in the catalytic reaction, in such a way that the presence of **O₂N-BZM9** more efficiently decreases the activity of the enzyme than **O₂N-BZM7**.

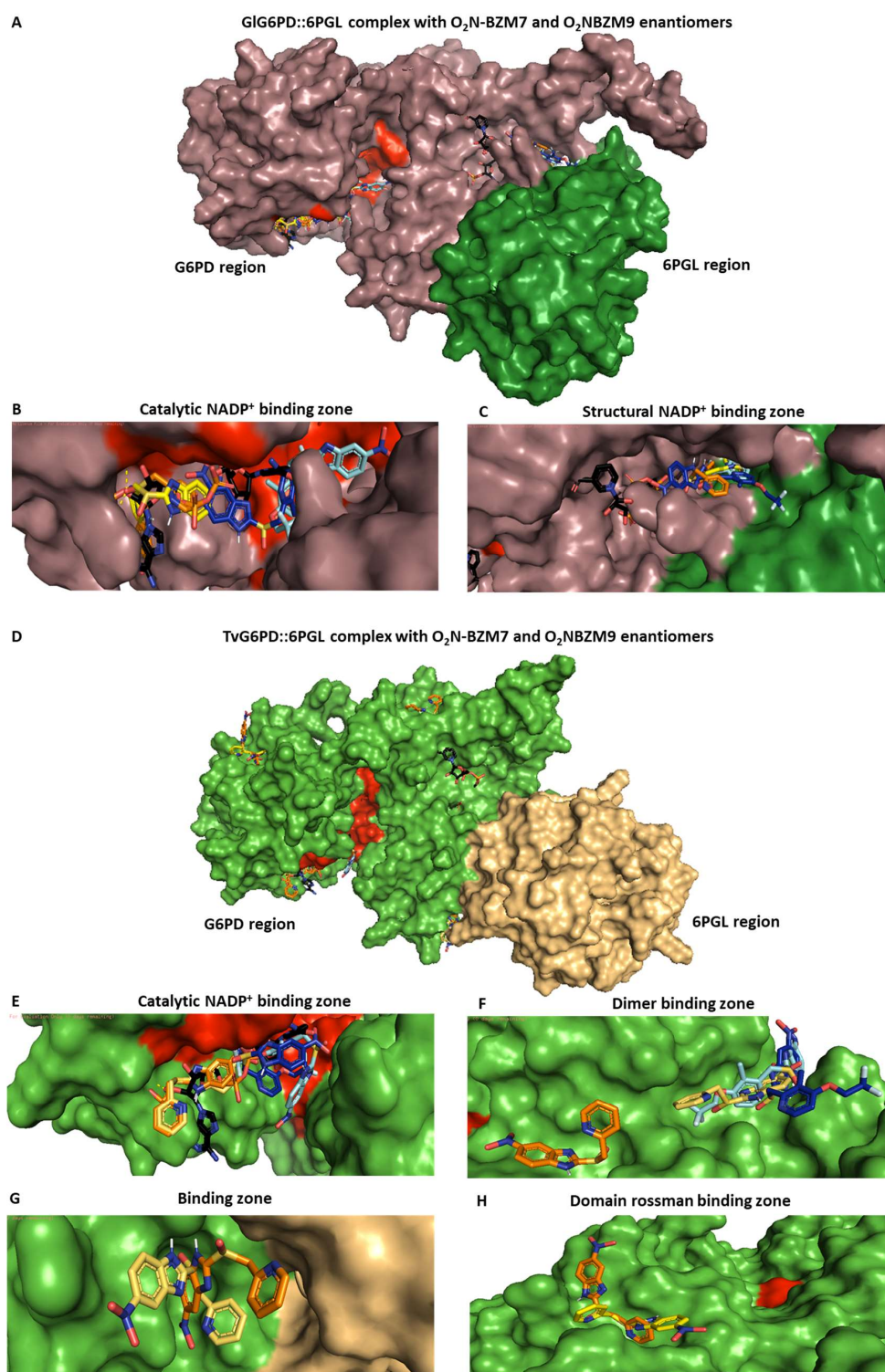


Figure 7. Prediction of the interaction zones between the O₂N-BZM7 and O₂N-BZM9 enantiomers and the GIG6PD::6PGL and TvG6Pd::6PGL proteins. (A) Closer view of the binding sites of O₂N-BZM7 and O₂N-BZM9 with GIG6PD::6PGL, (B) catalytic NADP⁺ binding, and (C) structural NADP⁺ binding site zones. (D) Closer view of the binding sites of O₂N-BZM7 and O₂N-BZM9 with TvG6PD::6PGL, (E) catalytic NADP⁺ binding, (F) dimer binding zone, (G) binding zone, and (H) domain Rossman binding zone. The NADP⁺ molecule is shown in black, and (R)-O₂N-BZM7, (S)-O₂N-BZM7, (R)-O₂N-BZM9, and (S)-O₂N-BZM9 are shown in orange, yellow, light blue, and dark blue, respectively.

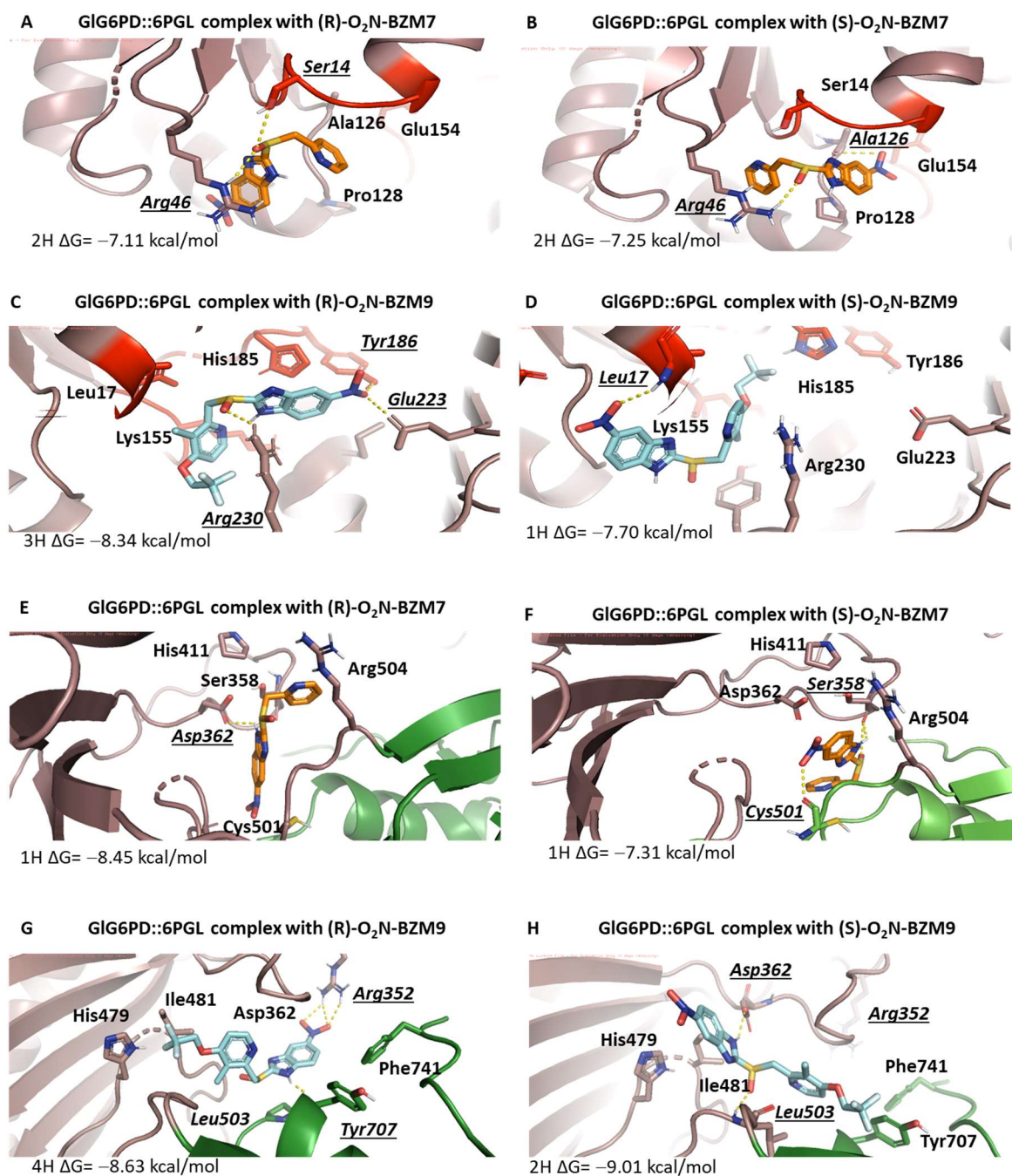


Figure 8. Interaction zones of the chemical compounds O₂N-BZM7 and O₂N-BZM9 on the GIG6PD::6PGL protein. (A) Interaction between the residues of the NADP⁺ catalytic site of GIG6PD::6PGL in the presence of (R)-O₂N-BZM7, (B) (S)-O₂N-BZM7, (C) (R)-O₂N-BZM9, and (D) (S)-O₂N-BZM9. (E) Interaction between the residues of the NADP⁺ structural site of GIG6PD::6PGL in the presence of (R)-O₂N-BZM7, (F) (S)-O₂N-BZM7, (G) (R)-O₂N-BZM9, and (H) (S)-O₂N-BZM9. The O₂N-BZM7 and O₂N-BZM9 compounds are shown in orange and light blue, respectively. H-bonds are represented in italic and underlined.

The docking of TvG6PD::6PGL and (R), (S)-O₂N-BZM7 revealed four probable zones of interaction (Figure 7D), whose the most stable zone corresponds to the region where the dimer is formed with a binding energy of -6.58 kcal/mol, where 44% of the conformers were found and the formation of a hydrogen bond between the nitro group and Asn203 occurred (Figure 9A). The second most probable zone is found in the 453-LKDKYPEI-460 loop; this loop is close to the 6PGL domain, with a binding energy of -7.24 kcal/mol, and

22% of the conformers were found in this zone (Figure 9C). The third zone corresponds to a zone close to the Rossman-type domain of the G6PD monomer with 19% of the population of conformers (a closer view is seen Figure 7H), and the zone where 16% of the conformers were bound corresponds to the catalytic NADP⁺ binding site (an overview is shown in Figure 7E). On the other hand, docking with (R)-O₂N-BZM9 showed that this ligand binds two zones of the TvG6PD::6PGL enzyme, where the largest population of conformers was found, corresponding to the zone near the catalytic NADP⁺, with a binding energy of −7.56 kcal/mol, where (R)-O₂N-BZM9 formed an H-bond with the sulfoxide group and Arg239 (Figure 9E). Lastly, the other zone was the near the binding site of catalytic NADP⁺ with a binding energy of −7.81 kcal/mol, and the ligand formed one H-bond between benzimidazole ring and Asp357 and one H-bond with the nitro group and Asn221 (Figure 9G). Similar results were found with the (S) enantiomer of O₂N-BZM7 and O₂N-BZM9 compounds (Figure 9B,D,F,H). These results are related to the in vitro inhibition studies that were carried out with the recombinant enzyme of *T. vaginalis*, where O₂N-BZM7 revealed a k_2 value of 0.85 M^{−1}·s^{−1}, while O₂N-BZM9 had a k_2 value of 1.62 M^{−1}·s^{−1}. This indicates that the O₂N-BZM9 compound forms a TvG6PD::6PGL-inhibitor complex more quickly. Moreover, structural, and biochemical studies showed that O₂N-BZM9 affects the tertiary structure of the enzyme to a greater extent, decreasing 84% of intrinsic protein fluorescence with respect to native proteins, while O₂N-BZM7 led to a 30% reduction.

2.5. In Vitro Assays over *T. vaginalis* Trophozoites

The screening for the trichomonocidal activities of O₂N-BZM7 and O₂N-BZM9 using a wider range of concentrations showed the potential for compounds to reduce trophozoite viability by 100% at 100 μM after 24 h relative to the negative control. As expected, the 0.06% DMSO control did not affect trophozoite viability, motility, and morphology (trophozoites do not stain with trypan blue). The O₂N-BZM7 and O₂N-BZM9 compounds similarly affected trophozoite, reducing their viability by 52% at 6 μM, while 100% viability was lost at a concentration of 100 μM (Figure 10). Overall, the compounds decreased the number of trophozoites in strains of *T. vaginalis* in a dose-dependent manner. Thus, IC₅₀ was determined as 6 μM and 4 μM for O₂N-BZM7 and O₂N-BZM9, respectively. These values determined for *T. vaginalis* are lower than those determined for *G. lamblia* (Table 3), since, in a previous study, IC₅₀ values of 14 μM and 17 μM were determined for O₂N-BZM7 and O₂N-BZM9, respectively [11]. In addition, metronidazole, a drug currently used to treat giardiasis and trichomoniasis, was used as a positive control. As shown in Table 3, IC₅₀ values of 12 μM and 4.8 μM were determined for *T. vaginalis* and *G. lamblia*, respectively. It is important to mention that O₂N-BZM7 and O₂N-BZM9 showed a lower IC₅₀ value than metronidazole in *T. vaginalis*, while, in *G. lamblia*, metronidazole showed a lower IC₅₀ value than the O₂N-BZM7 and O₂N-BZM9 compounds. Furthermore, the selectivity index (SI) demonstrates the differential activity of a pure compound: the greater the SI value, the more selective it is; thus, it is desirable to have a high SI, providing maximum anti-giardial and trichomonocidal activities with minimal cell toxicity. On the basis of the SI, the data shown in Table 3 indicate that the compounds exhibit a high degree of selective toxicity in *G. lamblia* and *T. vaginalis* compared to metronidazole. We propose that O₂N-BZM7 and O₂N-BZM9 are considered for follow-up as anti-giardial and trichomonocidal candidates with minimal cell toxicity.

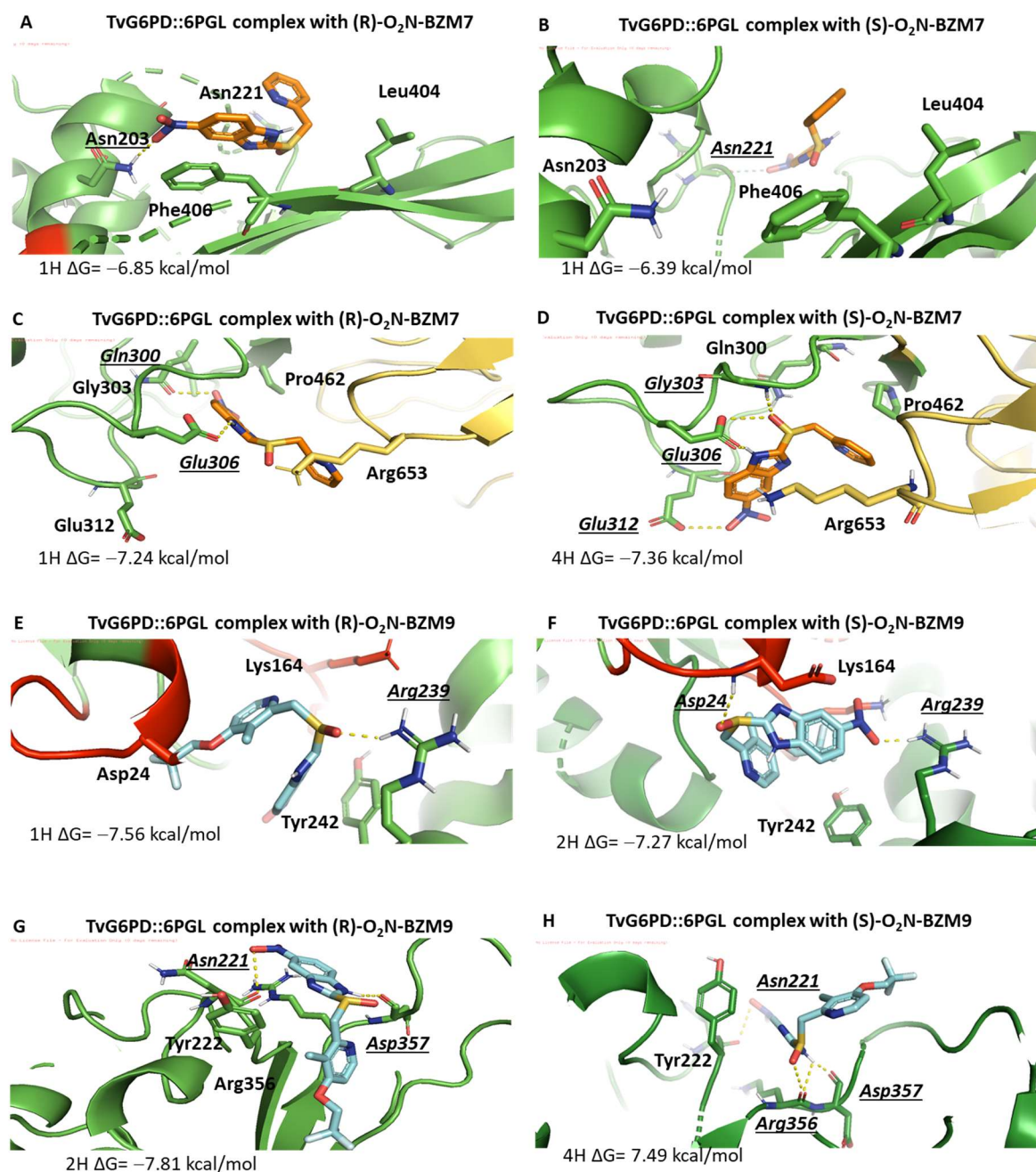


Figure 9. Interaction zones of the chemical compounds O₂N-BZM7 and O₂N-BZM9 in the TvG6PD::6PGL protein. (A) Interaction zone near the structural NADP⁺ site (R)-O₂N-BZM7, (B) (S)-O₂N-BZM7, and (C) the 6PGL domain of TvG6PD::6PGL with the compound (R)-O₂N-BZM7 and (D) (S)-O₂N-BZM7. (E) Close view in the NADP⁺ catalytic site of the (R)-O₂N-BZM9 and (F) (S)-O₂N-BZM9. (G) Interaction of the (R)-O₂N-BZM9, and (H) (S)-O₂N-BZM9 compound with residues close to the structural NADP⁺ site. The O₂N-BZM7 and O₂N-BZM9 compounds are shown in orange and light blue, respectively. H-bonds are represented in italic and underlined.

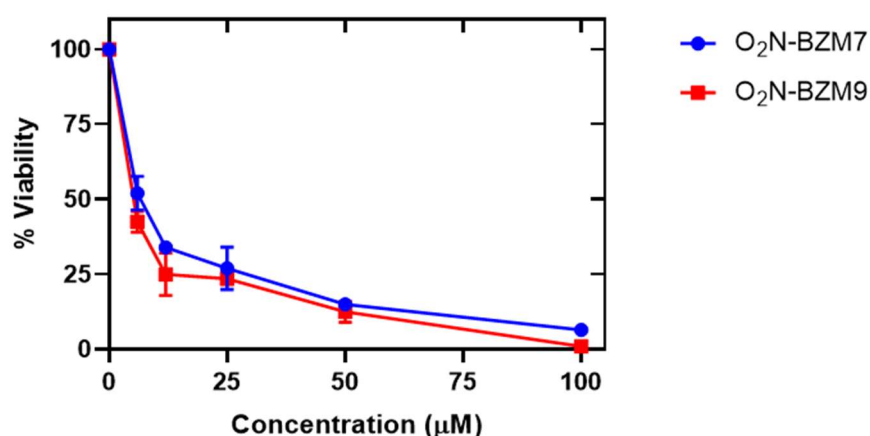


Figure 10. Antitrichomonal activity of the O₂N-BZM7 and O₂N-BZM9 compounds on *T. vaginalis* trophozoites' viability. The trophozoites were incubated in the presence of compounds, by 24 h at 37 °C with increasing concentrations of each of the compounds, and the viability of the trophozoites was later determined. The values represent the mean ± standard deviation from three independent experiments; standard errors were lower than 5%.

Table 3. In vitro anti-giardial and antitrichomonal activities of compounds, and the cytotoxic activity on Caco-2 cells.

Compound	O ₂ N-BZM7 µM (SI)	O ₂ N-BZM9 µM (SI)	Metronidazole µM (SI)
<i>T. vaginalis</i> IC ₅₀	6 (106)	4 (160)	12 (1.6)
<i>G. lamblia</i> IC ₅₀	14 (45)	17 (39)	4.8 (3.9)
Caco-2 (SI) CC ₅₀	640	663	19 [19]

T. vaginalis is the most common curable sexually transmitted disease worldwide, with a high incidence in women of reproductive age. However, persistent and recurrent infections by *T. vaginalis* are frequent, possibly due to the lack of timely diagnosis for this pathogen, as well as its resistance to prescription drugs [20]. Metronidazole and tinidazole are just two oral drugs that are used against trichomoniasis; hence, treatment options are lacking [21,22]. Several mechanisms may play a role in metronidazole resistance, including a decreased ability to reduce and activate 5-nitro-type prodrugs [23] with the detoxification of nitro radicals from the drug [24]. Therefore, the development of new agents suitable for the treatment of *T. vaginalis* is needed. There are several studies that support the efficacy of some compounds on *T. vaginalis*, such as ceragenins (cationic steroid antimicrobials compounds). However, with effective concentrations of 50 and 100 µM [25]. The other compounds are 2,8-bis(trifluoromethyl) quinoline analogs (QDA-1 and QDA-2) with an IC₅₀ of 113.8 µM [26] and *N*-acylhydrazones derivatives [27]; two of them had IC₅₀ values of 1.69 µM and 1.98 µM. These last compounds, as well as the O₂N-BZM7 and O₂N-BZM9 compounds proposed in this study, are promising antiparasitic compounds, since our results generally demonstrate the potential of O₂N-BZM7 and O₂N-BZM9 to affect both the enzymatic activity of TvG6PD::6PGL and the viability of *T. vaginalis* trophozoites, establishing a basis upon which to propose O₂N-BZM7 and O₂N-BZM9 as possible antitrichomonal and anti-giardial drugs.

2.6. Pharmacokinetic Predictive Values

The physicochemical characteristics of drugs affect both the rate and the magnitude of absorption. Once the drug is dissolved in the fluids of the intestinal lumen, several physicochemical factors have a strong influence on its passive absorption, such as lipophilic-

ity, solubility, pKa, and molecular size [28,29]. Therefore, a prediction of the absorption, distribution, metabolism, excretion, and toxicity (ADMET) parameters of compounds **O₂N-BZM7** and **O₂N-BZM9** was made using the platform ADMETLab 2.0 [30].

The in silico calculation, shown in Table 4, demonstrated that both compounds present high values of intestinal absorption, and only compound **O₂N-BZM9** is able to cross the blood-brain barrier (BBB). The absorption parameters, using the MDCK (Madin–Darby canine kidney) and Caco-2 as predictive models of intestinal drug absorption, indicate that the compounds have a high passive permeability. The distribution parameters calculated were plasma protein binding and the volume of distribution. Both compounds present optimal values of distribution, the optimal plasma protein binding is less than 95%, the **O₂N-BZM7** compound meets this parameter.

Table 4. Pharmacokinetic predictive values calculated with ADMETLab 2.0 for compounds **O₂N-BZM7** and **O₂N-BZM9**.

		Compounds		
	Model	O ₂ N–BZM7	O ₂ N–BZM9	Comments
A	Human intestinal absorption	(+) High	(+) High	Optimal: higher than –5.15 log units High passive permeability: >2.0 × 10 ^{–5} cm/s
	Caco-2 permeability	–4.509	–4.562	
	MDCK permeability	0.00025	0.00018	
	Bioavailability (F)	>30%	>30%	
D	Volume distribution	0.338 L/kg	0.358 L/kg	Optimal: 0.04–20 L/kg Probability of being BBB+ Optimal: <95%.
	BBB penetration	0.572	++	
	Plasma protein binding	94	100	
M	CYP2C19 substrate	(+) Yes	(+) Yes	Probability of inhibition/blockage
	CYP2C19 inhibitor	0.202	0.204	
	CYP3A4 substrate	(+) Yes	(+) Yes	
	CYP3A4 inhibitor	0.23	0.21	
E	Clearance (Cl)	2.908	4.026	mL/min/kg
	Half-life (T _{1/2})	>3 h	>3 h	
T	hERG blockers	0.024 inactive	0.018	Probability of inhibition
	Rat oral acute toxicity	–	–	

The oxidative metabolism by cytochrome P450 enzymes is the primary method used for the hepatic metabolism of drugs. The CYP2C19 and CYP3A4 isoforms participate in the metabolism of omeprazole [31]; therefore, the metabolic stability could be predicted, and compounds **O₂N-BZM7** and **O₂N-BZM9** are substrates of CYP2C19 and CYP3A4 isoforms. The excretion parameters were predicted, with the compounds showing satisfactory values of clearance and long half-lives (>3 h). Lastly, the toxicity parameters showed that the two main isoforms of CYP450 for **O₂N-BZM7** and **O₂N-BZM9** compounds showed low probabilities of being inhibited; therefore, the drug–drug interactions and undesirable adverse effects are likely to be low. Additionally, the compounds showed a very low prediction of hERG channel blockage and were considered non-cardiotoxic molecules (Table 4).

3. Materials and Methods

3.1. Purification of Fused GIG6PD::6PGL and TvG6PD::6PGL Recombinant Proteins

The recombinant GIG6PD::6PGL and TvG6PD::6PGL proteins were expressed in the *E. coli* BL21(DE3)pLysS strain containing the plasmid pET3a-HisTEVP, which was cloned using the *g6pd::6pgl* gene from both *G. lamblia* and *T. vaginalis* [14,32]. The bacterial culture was grown in 2 L of Luria–Bertani (LB) medium supplemented with 100 µg/mL ampicillin (Sigma Aldrich, St. Louis, MO, USA) and kanamycin (50 µg/mL) for 12 h at 37 °C and 160 rpm. Thereafter, 0.3 mM of isopropyl-β-D-thiogalactoside (IPTG) was added to the

culture at an optical density (OD 600 nm) of 0.8. The cells were pelleted by centrifugation, suspended in lysis buffer, and disrupted by sonication, as previously conducted by Morales-Luna et al. [14,30]. The crude extract was obtained by centrifugation at $10,000\times g$ for 30 min at 4 °C, and the clear supernatants were incubated with a previously equilibrated Ni Sepharose high-performance column (equilibrium buffer: 50 mM KH_2PO_4 , 150 mM NaCl, 5 μM NADP^+ , 2 mM DTT, and glycerol 10%; pH 7.35). The proteins were eluted with the same equilibrium buffer supplemented with 250 mM imidazole [14,32]. Then, the imidazole was removed from the proteins by consecutive dilutions using a microcon 10 kDa centrifugal filter unit (Millipore, Burlington, MA, USA). The purified proteins were digested with the Tobacco Etch Virus Protease (TEVP) to remove the (His)₆-tag sequence located in the *N*-terminal region of both proteins. The purity of GIG6PD::6PGL and TvG6PD::6PGL proteins was analyzed by 12% SDS-PAGE gels and stained with colloidal Coomassie blue (R-250) (Sigma Aldrich, St. Louis, MO, USA). The purified proteins were used to perform both functional and structural assays in the presence and absence of selected hit compounds.

3.2. Activity Assay

The G6PD domain activity of the recombinant proteins was spectrophotometrically measured at 25 °C by monitoring the reduction in NADP^+ at 340 nm [13]. The assay was performed with 1 mL of standard reaction mixture containing 0.1 M Tris-HCl, 0.01 M MgCl_2 , 1 mM NADP^+ , and 1 mM glucose-6-phosphate (G6P) at pH 8.3. The reaction was initiated with the addition of 1 $\mu\text{g}/\text{mL}$ fused GIG6PD::6PGL or TvG6PD::6PGL enzymes.

3.2.1. General Methodology for the Synthesis of Compounds

The five compounds were synthesized following a previously reported methodology, and the spectroscopic signals were accordingly with those previously published [11]. Briefly, the synthesis was carried out in two steps: first, the precursors were prepared with a mixture of 2-mercapto-5-benzimidazole and the substituted 2-chloromethyl pyridine in 1,2-dimethoxyethane (GLIMA) as the solvent and an alkaline medium (NaOH); the mixture was stirred for 8 h at 50 °C. The reaction was monitored by thin-layer chromatography (TLC) assay. The reaction mixture was extracted with CHCl_3 (2×20 mL). The organic layer was dried over anhydrous Na_2SO_4 and concentrated under reduced pressure, and the residue was purified using column chromatography on silica gel, with CH_2Cl_2 -hexane (3:1 *v/v*) as the eluent to give a pale-yellow solid. Second, the oxidation of the thioether group in precursors was carried out with 3-chloroperoxybenzoic acid and CHCl_3 as a solvent; the peracid was added slowly, and the reaction was monitored every 5 min by TLC. After completion of the reaction, the mixture was treated with a saturated solution of sodium bicarbonate and extracted with CHCl_3 (2×20 mL). The organic layer was dried over anhydrous Na_2SO_4 , and the solvent was removed under reduced pressure. The residue was purified by means of column chromatography.

3.2.2. Determination of the Molar Extinction Coefficient of the Compounds

Each compound's stock solutions were prepared to determine the compounds' molar extinction coefficient (ϵ). Solutions for the spectroscopic measurements were prepared by immediately dissolving accurately weighed amounts of compounds in the appropriate solvent volume before running the spectra. The absorption spectra were recorded on a Cary 100 Bio UV/visible spectrophotometer (Walnut Creek, CA, USA) using a rectangular quartz cuvette with a path length of 1 cm, and an absorbance scan was performed in the wavelength range of 190 to 600 nm. To determine the ϵ of each compound, we worked with a group of solutions with concentrations of 5, 10, 20, 30, and 40 mg/mL, a range in which the changes in absorbance was linear ($r = 0.9989$). This allowed obtaining the absorbance results at a concentration of 1 mg/mL and obtaining the coefficients (Table 5).

Table 5. UV molar extinction coefficients of compounds in aqueous phase. Percentage relative error < 5%.

Compound	Formula Weight (g/mol)	λ_{\max} (nm)	ϵ ($M^{-1}\cdot\text{cm}^{-1}$)
H-BZM1	257.31	299	15,456
H-BZM2	315.39	299	17,304
H ₂ N-BZM6	384.37	306	13,790
O ₂ N-BZM7	302.30	345	17,599
O ₂ N-BZM9	414.35	345	14,369

3.3. In Vitro Screening of GIG6PD::6PGL and TvG6PD::6PGL Inactivation with Compounds

Inactivation assays were performed with the compounds against GIG6PD::6PGL and TvG6PD::6PGL. Thus, all the compounds were activate immediately before the experiments as previously reported [3] and diluted using dimethyl sulfoxide (DMSO) as a solvent. For the assay, 0.2 mg/mL of the enzyme was incubated with the compounds at a concentration of 400 μM at 37 °C for 2 h. Following incubation, the activity was measured with a standard reaction mixture. Only the compounds that reduced the activity of the enzyme by more than 50% were used in the subsequent experiments.

The 50% inhibitory concentration (IC_{50}) values of the H-BZM2, O₂N-BZM7, and O₂N-BZM9 compounds against the fused enzymes from *G. lamblia* and *T. vaginalis* were established under the same conditions described above, with 0.2 mg/mL of the enzymes exposed for 2 h at compound concentrations ranging from 12 μM to 200 μM in TE buffer by 2 h at 25 °C. DMSO was maintained at 5% during incubation because this concentration did not affect the enzyme activity of both proteins. Then, aliquots from these incubations were withdrawn, and the residual activity was determined under standard conditions. The results are reported as the percentage of residual activity (using the activity of each enzyme incubated without any compound as 100% activity) versus the compound's concentration.

3.4. Second-Order Rate Constant (k_2) of Selected Hit Compounds

The second-order rate constants of inactivation for each one of the compounds were calculated by obtaining the pseudo-first-order rate constant (k_1) values. Pseudo-first-order inactivation rate constants (k_1) were obtained at four or five fixed concentrations for each of the compounds. At the indicated times, aliquots were withdrawn to determine residual activity. Then, residual activity data were fitted using the monoexponential decay equation, as previously reported [11,13]. The previously obtained k_1 values were replotted against the concentrations of each compound, and the slope created by these plots corresponds to the second-order inactivation constant k_2 ($M^{-1}\cdot s^{-1}$).

3.5. Spectroscopic and Chromatographic Characterization

3.5.1. Circular Dichroism Experiments

To determine whether compounds caused changes in the secondary structure of the GIG6PD::6PGL and TvG6PD::6PGL proteins, we performed circular dichroism (CD) assays using a Jasco-810 spectropolarimeter (Jasco J-810[®], Inc., Easton, MD, USA). Both proteins were adjusted at a protein concentration of 0.5 mg/mL with buffer P (50 mM phosphate, pH 7.35) and incubated for 2 h at 37 °C in the presence of the chemical compounds (IC_{50} of each compound). One control containing only enzyme was used in each assay. Then, the proteins were loaded in a quartz cell with a 0.1 cm path length, and spectral scans were recorded at 25 °C in ultraviolet circular dichroism (UV-CD) ranging from 200 to 260 nm. The spectra of the blanks (buffer P solution containing each of the compounds) were subtracted from all the obtained spectra that contained the protein. All the CD data were reported as molar ellipticity. The experiments were performed in triplicate.

3.5.2. Intrinsic Fluorescence Assays

The effect of the compounds on the tertiary structure (3D) of the GIG6PD::6PGL and TvG6PD::6PGL proteins was evaluated by monitoring the changes in the intrinsic

and extrinsic fluorescence using a Perkin-Elmer LS-55 spectrofluorometer (Perkin-Elmer, Wellesley, MA, USA). Both proteins were adjusted at 0.1 mg/mL in buffer P (50 mM phosphate, pH 7.35) and incubated with the IC₅₀ concentration of the two synthesized benzimidazole compounds for 2 h at 37 °C. Following incubation, the proteins were excited at 280 nm, and we recorded the emission spectra from 310 to 500 nm with a scan speed of 150 nm/min using excitation and emission slits of 4 and 8 nm, respectively. The spectra of the blanks (buffer phosphate containing each of the compounds) were subtracted from all the obtained spectra that contained the protein, and the spectrum of the enzyme without the compound was used as control. The final spectrum for each compound was the average of five scans.

3.5.3. Oligomeric Status of the Recombinant Proteins

To evaluate changes in the quaternary structure of the GIG6PD::6PGL and TvG6PD::6PGL proteins produced for the chemical compounds, a gel filtration column (GFC) analysis was performed. The proteins were adjusted at a final concentration of 0.5 mg/mL and incubated for 2 h at 37 °C with each one of the compounds. Then, the proteins were loaded on a Sephacryl TMS-200 HR HiPrep™ (16/60) gel filtration column (GE Healthcare, Chicago, IL, USA) previously equilibrated with phosphate buffer (50 mM pH 7.35) and coupled to the AKTA pure FPLC system (GE Healthcare). The same buffer was used as the mobile phase with a flow rate of 0.5 mL·min⁻¹, while monitoring the absorbance at 280 nm (mUA). Moreover, the column was calibrated using a gel filtration standard kit (Bio-Rad, Tokyo, Japan). Both the proteins and the standard were performed in triplicate.

3.6. In Silico Docking Calculation

The protein–ligand docking simulation was performed using the docking web service SwissDock [33], which is based on the protein–ligand docking program, EADock DSS. The models generated by Morales-Luna et al. 2018 [14] and Martinez-Rosas et al. 2022 [13] were used for the assay. The atomic coordinates of the models were submitted to the PDBsum server (PDBsum-EMBL-EBI) [34] to add the hydrogens to the structure. To identify all interactions on the proteins, blind docking was performed using the SwissDock Server (<http://www.swissdock.ch/docking>, accessed on 23 June 2022). The ligand structures of O₂N-BZM7 and O₂N-BZM9 (R) and (S) enantiomers were generated with Avogadro software 1.2.0 Qt version 4.8.6, and energy-minimized by UCSF Chimera software [35] and later docked on the models GIG6PD::6PGL and TvG6PD::6PGL. SwissDock generates all possible binding modes for each ligand; the most favorable binding modes for a given pocket are clustered. The predictions file provided the Cluster Rank/Element Full Fitness and estimated binding free energy ΔG. After molecular docking, we analyzed the best calculated binding poses, and the graphical representations were performed by PyMol Molecular Graphics System software (version 2.5.0, Schrödinger, LLC, New York, NY, USA).

3.7. In Vitro Assays over *T. vaginalis* Trophozoites

3.7.1. *T. vaginalis* Culture

The isolate *T. vaginalis*, Donne ATCC 30236 was axenically grown in trypticase–yeast extract–maltose (TYM) medium (pH 6.0), supplemented with 10% sterile horse serum (previously inactivated at 56 °C for 30 min), and incubated at 37 °C under microaerobic conditions [27,36]. The trophozoites were axenically maintained, and a trypan blue (0.4%) exclusion assay was performed to ensure that the minimum viability of 95% and logarithmic growth phase were achieved before proceeding to the antiparasitic assay.

3.7.2. Anti-*T. vaginalis* Assay

Drug susceptibility assays were performed to analyze the trichomonacidal potential of O₂N-BZM7 and O₂N-BZM9 compounds against *T. vaginalis*, as previously described [27].

The compounds were diluted in dimethylsulfoxide (DMSO) as a vehicle for solubilization. The 50% inhibitory concentration (IC_{50}) values against *T. vaginalis* were established with trophozoites exposed to benzimidazolic compounds for 24 h, with concentrations ranging from 6 μ M to 100 μ M. Trophozoites were adjusted to an initial density of 2.6×10^5 trophozoites/mL of TYM medium. Then, 1.5 mL tubes were seeded with 150 mL of *T. vaginalis* trophozoites/tubes (2.6×10^5 trophozoites/mL), **O₂N-BZM7** and **O₂N-BZM9** were added, and tubes were incubated at 37 °C with 5% CO₂ for 24 h. After incubation, trophozoites were counted with trypan blue (0.4%) (1:1, v/v) on a Neubauer chamber to determine the trophozoites' motility, morphology, and viability. Three controls were used in each assay: a negative control containing only trophozoites, a 0.06% DMSO control, and a positive control containing MTZ at 100 μ M (Sigma-Aldrich, St. Louis, MO, USA). The IC_{50} was calculated using the GraphPad Prism 8.0 software Inc. version 8.0.2 (263) (San Diego, CA, USA).

4. Conclusions

The **O₂N-BZM7** and **O₂N-BZM9** compounds can inactivate the G6PD::6PGL enzyme from *G. lamblia* (GIG6PD::6PGL) and *T. vaginalis* (TvG6PD::6PGL), showing higher inactivation constants in both enzymes and an alteration of its tertiary structure. The main characteristic of these compounds is that they have a nitro group in position 5 of the benzimidazole ring, unlike to omeprazole compound. Furthermore, **O₂N-BZM7** does not have substituents on the pyridine ring, while **O₂N-BZM9** has a methyl and a trifluoroethoxy groups. According to the molecular docking findings, their nitro group was shown to be outstanding in the formation of hydrogen bonds with different amino acids of the G6PD domain. **O₂N-BZM9** has a more favorable binding energy than **O₂N-BZM7** due to its ability to form the enzyme–inhibitor complex more quickly than **O₂N-BZM7**. As it does not bind to cysteines in the G6PD domain, the inactivation of the G6PD::6PGL fused enzymes is another important mechanism that is not found in the triosephosphate isomerase from *G. lamblia*. These findings reinforce the proposal of **O₂N-BZM7** and **O₂N-BZM9** as possible anti-giardial and antitrichomonal drugs in clinical practice.

Author Contributions: B.H.-O., V.M.-R., L.M.-L., E.C.-J., L.M.R.-R., D.O.-C., Y.R.-G., A.G.-V., R.A.-E., S.E.-F., R.A.C.-R., N.C.-R., C.W.-B., I.B.-R. and S.G.-M., investigation, data curation, formal analysis, methodology, writing—original draft, and writing—review and editing; B.H.-O. and S.G.-M., software and supervision; B.H.-O., S.E.-F. and S.G.-M., funding acquisition; S.G.-M., project administration. All authors have read and agreed to the published version of the manuscript.

Funding: This research was funded by the E022 Program, National Institute of Pediatrics, Mexico City, Mexico (Recursos Fiscales para la Investigación). S.G.-M. was supported by INP 021/2022. E.C.-J. and B.H.-O. were supported by HIM/2019/036 SSA. 1595, and S.E.-F. was supported by CONACyT 259105.

Institutional Review Board Statement: Not applicable.

Informed Consent Statement: Not applicable.

Data Availability Statement: Not applicable.

Acknowledgments: This work was performed in partial fulfillment of the requirements of B.H.-O. in the Posgrado en Biomedicina y Biotecnología Molecular at the Instituto Politécnico Nacional. B.H.-O., L.M.-L. and V.M.-R., received support from CONACyT, Mexico. In addition, the authors are grateful for the technical assistance of Maria Jose Gomez-Gonzalez, Ximena Gomez-Gonzalez, Ana Gabriela Hernández-Ochoa, and Luis Daniel Bernal-Albarrán. Lastly, the authors thank Javier Gallegos Infante (Instituto de Fisiología Celular, UNAM) for assistance with the bibliographic materials.

Conflicts of Interest: The authors declare no conflict of interest.

Sample Availability: Samples of the compounds are available from the authors.

References

1. Theel, E.S.; Pritt, B.S. Parasites. *Microbiol. Spectr.* **2016**, *4*, DMIH2-0013-2015. [[CrossRef](#)] [[PubMed](#)]
2. Enríquez-Flores, S.; Rodríguez-Romero, A.; Hernández-Alcántara, G.; Oria-Hernández, J.; Gutiérrez-Castrellón, P.; Pérez-Hernández, G.; de la Mora-de la Mora, I.; Castillo-Villanueva, A.; García-Torres, I.; Méndez, S.T.; et al. Determining the molecular mechanism of inactivation by chemical modification of triosephosphate isomerase from the human parasite *Giardia lamblia*: A study for antiparasitic drug design. *Proteins* **2011**, *9*, 2711–2724. [[CrossRef](#)]
3. Reyes-Vivas, H.; de la Mora-de la Mora, I.; Castillo-Villanueva, A.; Yépez-Mulia, L.; Hernández-Alcántara, G.; Figueroa-Salazar, R.; García-Torres, I.; Gómez-Manzo, S.; Méndez, S.T.; Vanoye-Carlo, A.; et al. Giardial triosephosphate isomerase as possible target of the cytotoxic effect of omeprazole in *Giardia lamblia*. *Antimicrob. Agents Chemother.* **2014**, *12*, 7072–7082. [[CrossRef](#)] [[PubMed](#)]
4. García-Torres, I.; de la Mora-de la Mora, I.; Marcial-Quino, J.; Gómez-Manzo, S.; Vanoye-Carlo, A.; Navarrete-Vázquez, G.; Colín-Lozano, B.; Gutiérrez-Castrellón, P.; Sierra-Palacios, E.; López-Velázquez, G.; et al. Proton pump inhibitors drastically modify triosephosphate isomerase from *Giardia lamblia* at functional and structural levels, providing molecular leads in the design of new anti-giardiasis drugs. *Biochim. Biophys. Acta* **2016**, *1860*, 97–107. [[CrossRef](#)] [[PubMed](#)]
5. Vique-Sánchez, J.L.; Caro-Gómez, L.A.; Brieba, L.G.; Benítez-Cardoza, C.G. Developing a new drug against trichomoniasis, new inhibitory compounds of the protein triosephosphate isomerase. *Parasitol. Int.* **2020**, *76*, 102086. [[CrossRef](#)]
6. Benítez-Cardoza, C.G.; Brieba, L.G.; Arroyo, R.; Rojo-Domínguez, A.; Vique-Sánchez, J.L. Triosephosphate isomerase as a therapeutic target against trichomoniasis. *Mol. Biochem. Parasitol.* **2021**, *246*, 111413. [[CrossRef](#)]
7. Hua, Y.; Dai, X.; Xu, Y.; Xing, G.; Liu, H.; Lu, T.; Chen, Y.; Zhang, Y. Drug repositioning: Progress and challenges in drug discovery for various diseases. *Eur. J. Med. Chem.* **2022**, *234*, 114239. [[CrossRef](#)]
8. López-Velázquez, G.; Fernández-Lainez, C.; de la Mora-de la Mora, J.I.; Caudillo de la Portilla, D.; Reynoso-Robles, R.; González-Maciél, A.; Ridaaura, C.; García-Torres, I.; Gutiérrez-Castrellón, P.; Olivios-García, A.; et al. On the molecular and cellular effects of omeprazole to further support its effectiveness as an anti-giardial drug. *Sci. Rep.* **2019**, *9*, 8922. [[CrossRef](#)]
9. Pérez-Villanueva, J.; Romo-Mancillas, A.; Hernández-Campos, A.; Yépez-Mulia, L.; Hernández-Luis, F.; Castillo, R. Antiprotozoal activity of proton-pump inhibitors. *Bioorg. Med. Chem. Lett.* **2011**, *24*, 7351–7354. [[CrossRef](#)]
10. Hernández-Ochoa, B.; Navarrete-Vázquez, G.; Nava-Zuazo, C.; Castillo-Villanueva, A.; Méndez, S.T.; Torres-Arroyo, A.; Gómez-Manzo, S.; Marcial-Quino, J.; Ponce-Macotela, M.; Rufino-González, Y.; et al. Novel giardicidal compounds bearing proton pump inhibitor scaffold proceeding through triosephosphate isomerase inactivation. *Sci. Rep.* **2017**, *7*, 7810. [[CrossRef](#)]
11. Hernández-Ochoa, B.; Gómez-Manzo, S.; Sánchez-Carrillo, A.; Marcial-Quino, J.; Rocha-Ramírez, L.M.; Santos-Segura, A.; Ramírez-Nava, E.J.; Arreguin-Espinosa, R.; Cuevas-Cruz, M.; Méndez-Tenorio, A.; et al. Enhanced Anti-giardial Effect of Omeprazole Analog Benzimidazole Compounds. *Molecules* **2020**, *17*, 3979. [[CrossRef](#)] [[PubMed](#)]
12. Cartee, N.M.P.; Wang, M.M. Binding of omeprazole to protein targets identified by monoclonal antibodies. *PLoS. ONE* **2020**, *15*, e0239464. [[CrossRef](#)] [[PubMed](#)]
13. Martínez-Rosas, V.; Hernández-Ochoa, B.; Navarrete-Vázquez, G.; Martínez-Conde, C.; Gómez-Chávez, F.; Morales-Luna, L.; González-Valdez, A.; Arreguin-Espinosa, R.; Enríquez-Flores, S.; Pérez de la Cruz, V.; et al. Kinetic and Molecular Docking Studies to Determine the Effect of Inhibitors on the Activity and Structure of Fused G6PD::6PGL Protein from *Trichomonas vaginalis*. *Molecules* **2022**, *27*, 1174. [[CrossRef](#)] [[PubMed](#)]
14. Morales-Luna, L.; Serrano-Posada, H.; González-Valdez, A.; Ortega-Cuellar, D.; Vanoye-Carlo, A.; Hernández-Ochoa, B.; Sierra-Palacios, E.; Rufino-González, Y.; Castillo-Rodríguez, R.A.; Pérez de la Cruz, V.; et al. Biochemical Characterization and Structural Modeling of Fused Glucose-6-Phosphate Dehydrogenase-Phosphoglucosyltransferase from *Giardia lamblia*. *Int. J. Mol. Sci.* **2018**, *19*, 2518. [[CrossRef](#)] [[PubMed](#)]
15. Ramírez, D.; Caballero, J. Is It Reliable to Use Common Molecular Docking Methods for Comparing the Binding Affinities of Enantiomer Pairs for Their Protein Target? *Int. J. Mol. Sci.* **2016**, *17*, 525. [[CrossRef](#)]
16. Au, S.W.; Naylor, C.E.; Gover, S.; Vandeputte-Rutten, L.; Scopes, D.A.; Mason, P.J.; Luzzatto, L.; Lam, V.M.; Adams, M.J. Solution of the structure of tetrameric human glucose 6-phosphate dehydrogenase by molecular replacement. *Acta Crystallogr. Sect. D Biol. Crystallogr.* **1999**, *55*, 826–834. [[CrossRef](#)]
17. Bautista, J.M.; Mason, P.J.; Luzzatto, L. Human glucose-6-phosphate dehydrogenase Lysine 205 is dispensable for substrate binding but essential for catalysis. *FEBS Lett.* **1995**, *366*, 61–64. [[CrossRef](#)]
18. Kotaka, M.; Gover, S.; Vandeputte-Rutten, L.; Au, S.W.; Lam, V.M.; Adams, M.J. Structural studies of glucose-6-phosphate and NADP⁺ binding to human glucose-6-phosphate dehydrogenase. *Acta Crystallogr. D Biol. Crystallogr.* **2005**, *61*, 495–504. [[CrossRef](#)]
19. Abhari, F.M.; Pirestani, M.; Dalimi, A. Anti-amoebic activity of a cecropin-melittin hybrid peptide (CM11) against trophozoites of *Entamoeba histolytica*. *Wien. Klin. Wochenschr.* **2019**, *131*, 427–434. [[CrossRef](#)]
20. Seña, A.C.; Bachmann, L.H.; Hobbs, M.M. Persistent and recurrent *Trichomonas vaginalis* infections: Epidemiology, treatment and management considerations. *Expert Rev. Anti-Infect. Ther.* **2014**, *12*, 673–685. [[CrossRef](#)]
21. Upcroft, P.; Upcroft, J.A. Drug targets and mechanisms of resistance in the anaerobic protozoa. *Clin. Microbiol. Rev.* **2001**, *14*, 150–164. [[CrossRef](#)] [[PubMed](#)]
22. Moya, I.A.; Su, Z.; Honek, J.F. Current and future perspectives on the chemotherapy of the parasitic protozoa *Trichomonas vaginalis* and *Entamoeba histolytica*. *Future Med. Chem.* **2009**, *4*, 619–643. [[CrossRef](#)] [[PubMed](#)]

23. Leitsch, D.; Burgess, A.G.; Dunn, L.A.; Krauer, K.G.; Tan, K.; Duchêne, M.; Upcroft, P.; Eckmann, L.; Upcroft, J.A. Pyruvate:ferredoxin oxidoreductase and thioredoxin reductase are involved in 5-nitroimidazole activation while flavin metabolism is linked to 5-nitroimidazole resistance in *Giardia lamblia*. *J. Antimicrob. Chemother.* **2011**, *66*, 1756–1766. [[CrossRef](#)]
24. Pal, D.; Banerjee, S.; Cui, J.; Schwartz, A.; Ghosh, S.K.; Samuelson, J. Giardia, Entamoeba, and Trichomonas enzymes activate metronidazole (nitroreductases) and inactivate metronidazole (nitroimidazole reductases). *Antimicrob. Agents. Chemother.* **2009**, *53*, 458–464. [[CrossRef](#)] [[PubMed](#)]
25. Polat, Z.A.; Cetin, A.; Savage, P.B. Evaluation of the in vitro activity of ceragenins against *Trichomonas vaginalis*. *Acta Parasitol.* **2016**, *61*, 376–381. [[CrossRef](#)] [[PubMed](#)]
26. Alves, M.S.D.; Sena-Lopes, Â.; das Neves, R.N.; Casaril, A.M.; Domingues, M.; Birmann, P.T.; da Silva, E.T.; de Souza, M.V.N.; Savegnago, L.; Borsuk, S. In vitro and in silico trichomonacidal activity of 2,8-bis(trifluoromethyl) quinoline analogs against *Trichomonas vaginalis*. *Parasitol. Res.* **2022**, *121*, 2697–2711. [[CrossRef](#)]
27. Alves, M.S.D.; das Neves, R.N.; Sena-Lopes, Â.; Domingues, M.; Casaril, A.M.; Segatto, N.V.; Nogueira, T.C.M.; de Souza, M.V.N.; Savegnago, L.; Seixas, F.K.; et al. Antiparasitic activity of furanyl N-acylhydrazone derivatives against *Trichomonas vaginalis*: In vitro and in silico analyses. *Parasit. Vectors* **2020**, *13*, 59. [[CrossRef](#)]
28. Mannhold, R. The impact of lipophilicity in drug research: A case report on beta-blockers. *Mini Rev. Med. Chem.* **2005**, *5*, 197–205. [[CrossRef](#)]
29. Bergström, C.A. In silico predictions of drug solubility and permeability: Two rate-limiting barriers to oral drug absorption. *Basic Clin. Pharmacol. Toxicol.* **2005**, *96*, 156–161. [[CrossRef](#)]
30. Xiong, G.; Wu, Z.; Yi, J.; Fu, L.; Yang, Z.; Hsieh, C.; Yin, M.; Zeng, X.; Wu, C.; Lu, A.; et al. ADMETlab 2.0: An integrated online platform for accurate and comprehensive predictions of ADMET properties. *Nucleic Acids Res.* **2021**, *49*, W5–W14. [[CrossRef](#)]
31. Ogilvie, B.W.; Yerino, P.; Kazmi, F.; Buckley, D.B.; Rostami-Hodjegan, A.; Paris, B.L.; Toren, P.; Parkinson, A. The proton pump inhibitor, omeprazole, but not lansoprazole or pantoprazole, is a metabolism-dependent inhibitor of CYP2C19: Implications for coadministration with clopidogrel. *Drug. Metab. Dispos.* **2011**, *39*, 2020–2033. [[CrossRef](#)]
32. Morales-Luna, L.; Hernández-Ochoa, B.; Ramírez-Nava, E.J.; Martínez-Rosas, V.; Ortiz-Ramírez, P.; Fernández-Rosario, F.; González-Valdez, A.; Cárdenas-Rodríguez, N.; Serrano-Posada, H.; Centeno-Leija, S.; et al. Characterizing the Fused TvG6PD::6PGL Protein from the Protozoan *Trichomonas vaginalis*, and Effects of the NADP⁺ Molecule on Enzyme Stability. *Int. J. Mol. Sci.* **2020**, *21*, 4831. [[CrossRef](#)] [[PubMed](#)]
33. Grosdidier, A.; Zoete, V.; Michielin, O. SwissDock, a protein-small molecule docking web service based on EADock DSS. *Nucleic Acids Res.* **2011**, *39*, W270–W277. [[CrossRef](#)] [[PubMed](#)]
34. Laskowski, R.A.; Jabłońska, J.; Pravda, L.; Vařeková, R.S.; Thornton, J.M. PDBsum: Structural summaries of PDB entries. *Protein Sci.* **2018**, *27*, 129–134. [[CrossRef](#)] [[PubMed](#)]
35. Pettersen, E.F.; Goddard, T.D.; Huang, C.C.; Couch, G.S.; Greenblatt, D.M.; Meng, E.C.; Ferrin, T.E. UCSF Chimera—A visualization system for exploratory research and analysis. *J. Comput. Chem.* **2004**, *25*, 1605–1612. [[CrossRef](#)] [[PubMed](#)]
36. Diamond, L.S. The establishment of various trichomonads of animals and man in axenic cultures. *J. Parasitol.* **1957**, *43*, 488–490. [[CrossRef](#)]